

On the Ergodic Secrecy Capacity of Reconfigurable Intelligent Surface Aided Wireless Systems Under Mixture Gamma Fading

Alexandros-Apostolos A. Boulogeorgos*[†], and Angeliki Alexiou*

*Department of Digital Systems, University of Piraeus, Piraeus 18534, Greece,
E-mails: al.boulogeorgos@ieee.org, alexiou@unipi.gr

[†] Department of Electrical and Computer Engineering, University of Western Macedonia, Kozani, Greece

Abstract—This paper presents a quantified assessment of the physical layer security capabilities of reconfigurable intelligent surface (RIS)-aided wireless systems under eavesdropping. Specifically, we derive a closed-form expression for the ergodic secrecy capacity (ESC) that is adaptable to different types of fading and RIS size. The channels between the transmitter (TX) and RIS, the RIS and legitimate receiver as well as the TX and eavesdropper are assumed to follow independent mixture Gamma (MG) distributions. Note that MG is capable of modeling a large variety of well-known distributions, including Gaussian, Rayleigh, Nakagami- m , Rice, and others. The results reveal that as the RIS size increases, although the legitimate links diversity order increases, the ESC gain decreases.

Index Terms—Physical layer security, Reconfigurable intelligent surfaces, Secrecy capacity analysis, Theoretical framework.

I. INTRODUCTION

Reconfigurable intelligent surfaces (RISs) allow flexible manipulation of the propagation environment creating additional degrees of freedom, which in turn enables enhanced physical layer security (PLS) capabilities [1]–[11]. Inspired by this, a great amount of effort has been put on designing RIS phase shift (PS) selection strategies that maximizes the system’s secrecy capacity and theoretical frameworks that quantify the PLS capabilities of RIS-aided wireless systems.

From the RIS PS selection strategy design perception, the authors of [12] formulated and solved a secrecy capacity maximization problem through jointly designing the access point transmit and RIS reflect beam vectors in a RIS-aided secure wireless system, where a multi-antenna access point sends confidential messages to a single-antenna user in the presence of a single-antenna eavesdropper. In [13], the authors presented a joint power allocation and RIS PS design strategy that minimizes the transmit power subject to the secrecy capacity constraint at the legitimate user in RIS-aided wireless systems. In [14], a secrecy capacity maximization policy that accounts for the source transmit power and PS constraints at the RIS was documented. In [15], the design of robust, secure, and energy efficient transmission in RIS-aided wireless systems by jointly optimizing the transmission beam and RIS PS vectors as well as the artificial noise covariance matrix was reported. Finally, the authors of [16] studied the problem of

sum rate maximization without violating the PLS requirements of a RIS-aided multi-user cellular system by jointly designing the receive decoder at the end-users, the digital precoder and the artificial noise at the base station, as well as the PS at the RIS.

From the performance analysis point of view, in [17], the authors investigated the secrecy outage performance of a RIS-aided wireless system, in which both the legitimate user and the eavesdropper receive the information signal via the same RIS. In [18], an approximation of ergodic secrecy rate of RIS-aided wireless systems in the presence of eavesdropper was documented. The authors of [19] quantified the secrecy capacity performance of two-way RIS-aided wireless systems, assuming that all the established channels can be modeled as Rayleigh RVs. In [20], the authors reported a theoretical framework for the evaluation of secrecy outage probability and ergodic secrecy capacity in the presence of discrete phase noise. Finally, in [21], the authors quantified the secrecy outage performance of RIS-aided vehicle-to-vehicle and vehicle-to-infrastructure wireless systems, in which the eavesdropper establishes a direct link with the source, while no link between the RIS and the eavesdropper exists. All the aforementioned works assumed that all the established channels can be modeled as Rayleigh distributed random variables (RVs).

The secrecy performance of RIS-aided wireless systems are highly dependent on the statistics of the established communication channels. However, to the best of the authors knowledge, all the so far published contributions assumed that the established links experience Rayleigh fading. A general theoretical framework that accounts for different types of channels could serve as a useful tool for quantification of PLS capabilities of RIS-aided wireless systems in different propagation environments. Motivated by this, this contribution focuses on the investigation of the secrecy performance of such systems under different channel conditions. In more detail, we present a comprehensive system model in which the transmitter (TX) communicates with the legitimate user via an RIS, while the eavesdropper directly receives the information signal from the receiver. In contrast to previous publications, we assume mixture Gamma (MG) fading in both the TX to RIS and RIS to legitimate receiver (RX) as well as TX

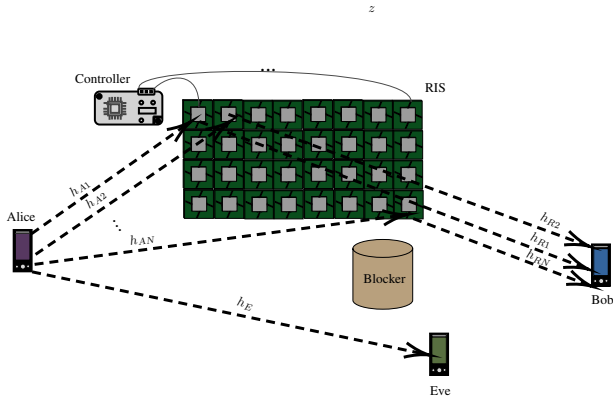


Fig. 1: System model.

to eavesdropper channels. Note that MG has been proven to be capable of accurate modeling an important number of fading conditions including but not limited to Rayleigh, Rice, Nakagami- m , Gamma, and generalized Gamma [22]. Building upon the aforementioned system model, we extract a novel theoretical framework for the quantification of the ergodic secrecy capacity of RIS-aided wireless system. This framework evaluates the PLS performance envelop and provides useful insights for the design of PLS in RIS-aided wireless systems.

Notations: Unless otherwise stated, the operators $\mathbb{E}[\cdot]$, $\exp(x)$, $\log_2(x)$ and $\ln(x)$ denote the statistical expectation, the exponential function, the base-2 logarithm of x , and the natural logarithm of x , respectively. Moreover, $K_n(x)$ stands for the modified Bessel function of the second kind and of the n -th order [23, Eq. (8.407)]. The upper incomplete Gamma functions [23, Eq. (8.350/2)] is represented by $\Gamma(\cdot, \cdot)$, respectively, while the Gamma function [23, Eq. (8.310)] is denoted by $\Gamma(\cdot)$. Finally, ${}_2F_1(\cdot, \cdot; \cdot; \cdot)$ stands for the Gauss hypergeometric function [24, Eq. (4.1.1)], while $G_{p,q}^{m,n} \left(x \left| \begin{matrix} a_1, a_2, \dots, a_p \\ b_1, b_2, \dots, b_q \end{matrix} \right. \right)$ denotes the Meijer's G-function [23, Eq. (9.301)].

II. SYSTEM AND SIGNAL MODEL

As illustrated in Fig. 1, we consider a RIS-aided wireless system that consists of a TX, a legitimate RX and an eavesdropper. In what follows, we refer to the TX as Alice, the legitimate RX as Bob and the eavesdropper as Eve. Alice, Bob and Eve are assumed to be equipped by a single antenna. The RIS has N meta-atoms (MAs) that are coordinated by a controller. No direct link can be established between Alice and Bob. Thus, Alice communicates with Bob through the RIS. The baseband equivalent received signal at Bob can be expressed as

$$r_B = \beta_B A s + n_B, \quad (1)$$

where s is Alice transmission symbol, n_B is a zero-mean Gaussian distributed RV with variance equal to N_o that models the additive white Gaussian noise (AWGN) and β_B stands for the end-to-end geometric gain, which depends on

the Bob's and Alice antenna gains, the RIS gain, the Bob-RIS and RIS-Alice distance, and the transmission frequency. Moreover, A denotes the Alice-RIS-Bob end-to-end-channel, which according to [25], can be evaluated as

$$A = \sum_{i=1}^N h_{A,i} g_i h_{R,i}, \quad (2)$$

where $h_{A,i}$ and $h_{R,i}$ are respectively the Alice- i -th MA and i -th MA-Bob channel coefficients. Likewise, g_i stands for the i -th MA response and can be obtained as

$$g_i = |g_i| \exp(j\phi_{g_i}), \quad (3)$$

with $|g_i|$ and ϕ_{g_i} being respectively the amplitude and phase of g_i . Let $\phi_{h_{A,i}}$ and $\phi_{h_{R,i}}$ respectively be the $h_{A,i}$ and $h_{R,i}$ phases. By assuming that the RIS controller has fully knowledge of $\phi_{h_{A,i}}$ and $\phi_{h_{R,i}}$ for all $i \in [1, N]$, the optimal phase response of the i -th MA can be obtained as

$$\phi_{g_i} = -\phi_{h_{A,i}} - \phi_{h_{R,i}}. \quad (4)$$

Without loss of generality, $|g_i| = 1$ for all $i \in [1, N]$. Thus, by applying (4) to (2), the Alice-RIS-Bob end-to-end channel can be expressed as

$$A = \sum_{i=1}^N |h_{A,i}| |h_{R,i}|. \quad (5)$$

Note that $|h_{A,i}|$ and $|h_{R,i}|$ are independent MG RVs with probability density functions (PDFs) that can be respectively expressed as

$$f_{h_{A,i}}(x) = \sum_{m=1}^M 2 a_m^{(1)} x^{2b_m^{(1)}-1} \exp(-c_1 x^2) \quad (6)$$

and

$$f_{h_{R,i}}(x) = \sum_{k=1}^K 2 a_k^{(2)} x^{2b_k^{(2)}-1} \exp(-c_2 x^2), \quad (7)$$

where M and K represents the numbers of terms that have been used to approximate the PDF of $|h_{A,i}|$ and $|h_{R,i}|$, respectively. Moreover, $a_m^{(1)}$ and $b_m^{(1)}$ with $m \in [1, M]$ and c_1 are parameters of the m -th term of (6). Finally, $a_k^{(2)}$ and $b_k^{(2)}$ with $k \in [1, K]$ and c_2 are parameters of the m -th term of (7).

By assuming that a direct link can be established between Alice and Eve and no-direct link exists between the RIS and Eve¹, the received baseband equivalent at Eve can be obtained as

$$r_E = \beta_E h_E s + n_E, \quad (8)$$

where n_E is a zero-mean Gaussian RV with variance N_o that models the AWGN. Additionally, β_E is the geometric gain

¹Note that this is considered a realistic assumption, since the RIS steer the incident beam towards Bob and not towards Eve; thus, Eve captures a very small fraction of the reflected power from a secondary RIS lobe, which is expected to be below the noise threshold. As a result, Eve can only receive signal directly from Alice [26]–[29].

of the Alice-Eve link. Moreover, h_E denotes the Alice-Eve channel fading coefficient. The envelop of h_E is modeled as a MG RV with PDF that can be written as

$$f_{h_E}(x) = \sum_{l=1}^L 2a_l^{(3)} x^{2b_l^{(3)}-1} \exp(-c_3 x^2), \quad (9)$$

where L denotes the number the numbers of terms employed to approximate the PDF of $|h_E|$. In addition, $a_l^{(3)}$, $b_l^{(3)}$ with $l \in [1, L]$ and c_3 are parameters of the l -th term of (9).

III. PERFORMANCE ANALYSIS

By assuming that the TX has only average channel state information (CSI) and no instantaneous CSI of either the legitimate nor eavesdropping links, the secrecy capacity is defined as

$$C_s = C_B - C_E. \quad (10)$$

where, C_B stands for the legitimate channel capacity that can be expressed as

$$C_B = \log_2(1 + \gamma_B), \quad (11)$$

with γ_B being the instantaneous signal-to-noise-ratio (SNR) at Bob. Notice, that, according to (10), the instantaneous secrecy capacity can take both negative and positive values. If the instantaneous secrecy capacity is positive, by selecting a suitable transmission data rate, physical layer security can be achieved. On the contrary, if $C_s \leq 0$, physical layer security cannot be achieved.

From (1), the instantaneous SNR at Bob can be obtained as

$$\gamma_B = \frac{\beta_B^2 A^2 P_s}{N_o}, \quad (12)$$

where P_s is Alice average transmission power. Similarly, C_E stands for the eavesdropping channel capacity, which can be analyzed as

$$C_E = \log_2(1 + \gamma_E), \quad (13)$$

where γ_E denotes the SNR at Eve. From (8), the instantaneous SNR at Eve can be expressed as

$$\gamma_E = \frac{\beta_E^2 |h_E|^2 P_s}{N_o}. \quad (14)$$

The following theorem returns a closed-form expressions for the ergodic secrecy capacity.

Theorem 1. *The ergodic secrecy capacity can be obtained as in (15), given at the top of the next page. In (15),*

$$k_A = -\frac{b_A}{2a_A} + \frac{\sqrt{b_A^2 - 4a_A c_A}}{2a_A}, \quad (16)$$

$$m_A = -\frac{b_A}{2a_A} - \frac{\sqrt{b_A^2 - 4a_A c_A}}{2a_A} \quad (17)$$

and

$$\Xi = \sqrt{\frac{k_A m_A}{\Omega_A}}. \quad (18)$$

In (16)–(18),

$$a_A = \mu_A(6) \mu_A(2) + (\mu_A(2))^2 \mu_A(4) - 2(\mu_A(4))^2, \quad (19)$$

$$b_A = \mu_A(6) \mu_A(2) - 4(\mu_A(4))^2 + 3(\mu_A(2))^2 \mu_A(4), \quad (20)$$

$$c_A = 2(\mu_A(2))^2 \mu_A(4) \quad (21)$$

and

$$\Omega_A = \mu_A(2), \quad (22)$$

where

$$\mu_A(l) = \sum_{l_1=0}^l \sum_{l_2=0}^{l_1} \cdots \sum_{l_{N-1}=0}^{l_{N-2}} \binom{l}{l_1} \binom{l_1}{l_2} \cdots \binom{l_{N-2}}{l_{N-1}} \times \mu_{\chi_1}(l-l_1) \mu_{\chi_2}(l_1-l_2) \cdots \mu_{\chi_{N-1}}(l_{N-1}) \quad (23)$$

and

$$\mu_{\chi_i}(l) = \sum_{m=1}^M \sum_{k=1}^K a_m^{(1)} a_k^{(2)} \left(\frac{c_1}{c_2}\right)^{-\frac{b_m^{(1)}-b_k^{(2)}}{2}} (c_1 c_2)^{-\frac{b_m^{(1)}+b_k^{(2)}+n}{2}} \times \Gamma\left(b_m^{(1)} + \frac{n}{2}\right) \Gamma\left(b_k^{(2)} + \frac{n}{2}\right) \quad (24)$$

Proof: For brevity, the proof is provided in the Appendix. ■

IV. RESULTS & DISCUSSION

This section focuses on verifying the theoretical framework by means of Monte Carlo simulations. The following scenario is considered. It is assumed that the Alice-RIS and RIS-Bob channel coefficients follow independent and identical Rice distributions with K_r parameter equal to 5 dB, while the Alice-Eve channel coefficient is modeled as a Nakagami- m RV with $m = 2$. For an accurate approximation of the Rice distribution, we select $M = K = 20$,

$$a_n^{(i)} = \frac{\delta(K_r, n)}{\sum_{k_1=1}^{N_r} \delta(K_r, k_1) \Gamma\left(b_{k_1}^{(2)}\right) c_i^{-b_{k_1}^{(i)}}}, \quad (25)$$

where $\delta(K_r, n) = \frac{K_r^{n-1}(1+K_r)^n}{\exp(K_r)((n-1)!)^2}$, while $c_i = 1 + K_r$, and $b_n^{(i)} = n$. Note that $i \in \{1, 2\}$ and

$$N_r = \begin{cases} M, & i = 1 \\ K, & i = 2 \end{cases}. \quad (26)$$

The MG distribution can be simplified to Nakagami- m by setting $L = 1$, $a_l^{(3)} = \frac{m^m}{\Gamma(m)}$, and $b_l^{(3)} = c_3 = m$ with m being the shape parameter.

Figure 2 depicts the ergodic secrecy capacity as a function of N for different values of β_E^2 , assuming that $\beta_B^2 = 0$. As expected, for a given N , as the eavesdropping channel improves, i.e. as β_E^2 increases, the ergodic secrecy capacity decreases. For example, for $N = 4$, the ergodic secrecy capacity decreases from 3.34 to 2.81 bits/s/Hz, as β_E^2 increases from -5 to 0 dB. In other words, a 15.9% ergodic secrecy capacity degradation is observed. Similarly, for $N = 8$, the ergodic secrecy capacity decreases from 5.33 to 4.78 bits/s/Hz, for the same β_E^2 increase. This is translated into a 10.2% ergodic

$$C_s = \frac{1}{\ln(2)} \left(\frac{\beta_B^2 P_s}{N_o} \right)^{-\frac{k_A+m_A}{2}} \frac{\Xi^{k_A+m_A}}{\Gamma(k_A)\Gamma(m_A)} G_{2,4}^{4,1} \left(\frac{\Xi^2 N_o}{\beta_B^2 P_s} \middle| \begin{matrix} -\frac{k_A+m_A}{2}, 1 - \frac{k_A+m_A}{2} \\ \frac{k_A-m_A}{2}, -\frac{k_A-m_A}{2}, -\frac{k_A+m_A}{2}, -\frac{k_A+m_A}{2} \end{matrix} \right) - \sum_{l=1}^L \frac{a_l^{(3)} c_3^{-b_l^{(3)}}}{\ln(2)} G_{4,3}^{1,4} \left(\frac{\beta_E^2 P_s}{c_3 N_o} \middle| \begin{matrix} 0, 0, 1 - b_l^{(3)}, -b_l^{(3)} \\ 0, -b_l^{(3)}, -1 \end{matrix} \right) \quad (15)$$

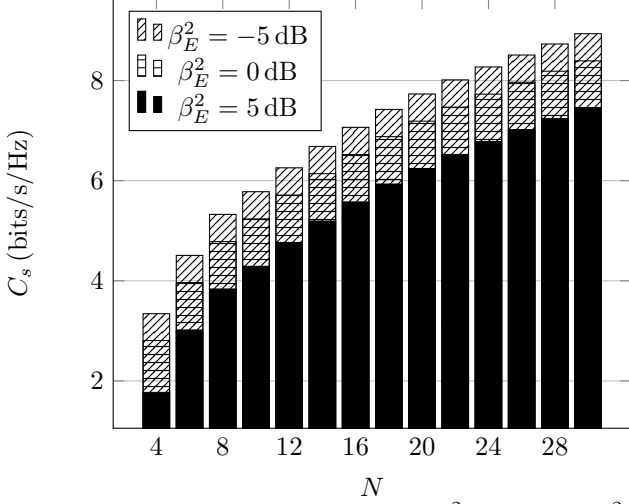


Fig. 2: C_s vs N for different values of β_E^2 , assuming $\beta_B^2 = 0$ dB.

secrecy capacity degradation. From these examples, it becomes evident that as N increases, the ergodic secrecy capacity degradation, due to eavesdropping channel improvement, decreases. Moreover, from this figure, it becomes apparent that, for a fixed β_E^2 , as N increases, the system's diversity order increases; thus, the ergodic secrecy capacity increases. For instance, for $\beta_E^2 = 0$ dB, the ergodic secrecy capacity increases from 2.81 to 3.96 bits/s/Hz as N increases from 4 to 6, and from 6.14 to 6.52 bits/s/Hz, as N increases from 14 to 16. This indicates that, although as N increases, the diversity order increases, the diversity gain to the ergodic secrecy capacity decreases.

Figure 3 illustrates the ergodic secrecy capacity as a function of β_B^2 , for different values of β_E^2 and N . We observe that for given β_E^2 and N , as β_B^2 increases, the legitimate channel improves; as a result, the ergodic secrecy capacity increases. For example, for $\beta_E^2 = 0$ dB and $N = 32$, the ergodic secrecy capacity increases from 5.28 to 8.59, as β_B^2 increases from -10 to 0 dB. Moreover, for fixed β_B^2 and N , as β_E^2 increases, the ergodic secrecy capacity decreases. For instance, for $\beta_B^2 = 0$ dB and $N = 32$, the ergodic secrecy capacity changes from 8.59 to 7.64 bits/s/Hz, as β_E^2 increases from 0 to 5 dB. Finally, for given β_B^2 and β_E^2 , as N increases, the diversity order and gain increase; hence the ergodic secrecy capacity increases.

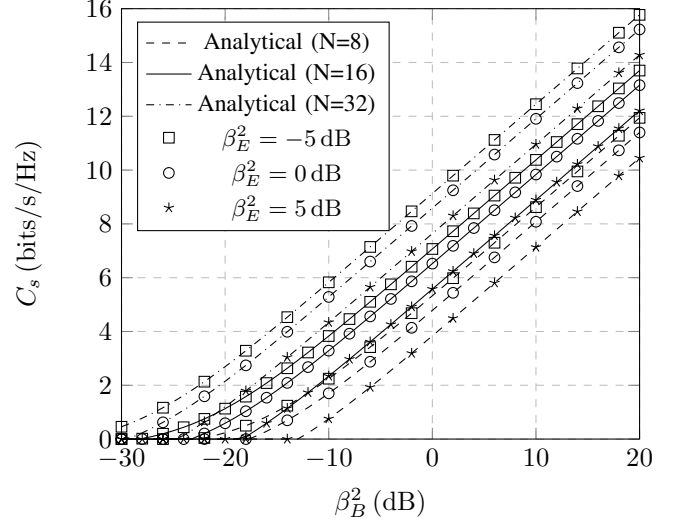


Fig. 3: C_s vs β_B^2 , for different values of β_E^2 and N .

V. CONCLUSIONS

In this paper, we investigated the PLS capabilities of RIS-aided wireless systems in the presence of eavesdropper. We derived a novel and general closed-form expression for the ergodic secrecy capacity that accounts for both different types of fading and different RIS sizes. The results highlighted that beyond a specific RIS size, i.e., number of RIS elements, a further increase of the RIS size will not result to important PLS capabilities improvements.

APPENDIX

PROOF OF THEOREM 1

Based on (10), the ergodic secrecy capacity can be evaluated as

$$\overline{C}_s = \mathbb{E}[C_s], \quad (27)$$

or

$$\overline{C}_s = \mathbb{E}[C_B - C_E], \quad (28)$$

or equivalently

$$\overline{C}_s = \overline{C}_B - \overline{C}_E, \quad (29)$$

where

$$\overline{C}_B = \mathbb{E}[C_B] \text{ and } \overline{C}_E = \mathbb{E}[C_E]. \quad (30)$$

are respectively the ergodic capacities of the legitimate and eavesdropping channels.

The ergodic capacity of the legitimate channel can be evaluated as

$$\bar{C}_B = \int_0^\infty \log_2 \left(1 + \frac{\beta_B^2 P_s}{N_o} x^2 \right) f_A(x) dx, \quad (31)$$

which, by applying [22, Eq.(17)], can be rewritten as

$$\bar{C}_B = \frac{4\Xi^{k_A+m_A}}{\Gamma(k_A)\Gamma(m_A)} \mathcal{J}, \quad (32)$$

where

$$\mathcal{J} = \int_0^\infty x^{k_A+m_A-1} \log_2 \left(1 + \frac{\beta_B^2 P_s}{N_o} x^2 \right) K_{k_A-m_A}(2\Xi x) dx. \quad (33)$$

To extract a closed-form expression for (33), we first employ [24, Eq. (15.1.1)], and rewrite (33) as

$$\mathcal{J} = \frac{\beta_B^2 P_s}{\ln(2) N_o} \int_0^\infty x^{k_A+m_A+1} {}_2F_1 \left(1, 1; 2; -\frac{\beta_B^2 P_s}{N_o} x^2 \right) \times K_{k_A-m_A}(2\Xi x) dx. \quad (34)$$

Next, by applying [23, Eq. (9.34/7)], we obtain

$$\mathcal{J} = \frac{\beta_B^2 P_s}{\ln(2) N_o} \int_0^\infty x^{k_A+m_A+1} G_{2,2}^{1,2} \left(\frac{\beta_B^2 P_s}{N_o} x^2 \mid \begin{matrix} 0, 0 \\ 0, -1 \end{matrix} \right) \times K_{k_A-m_A}(2\Xi x) dx, \quad (35)$$

which, with the aid of [30], can be rewritten as

$$\mathcal{J} = \frac{\beta_B^2 P_s}{2\ln(2) N_o} \int_0^\infty x^{k_A+m_A+1} G_{2,2}^{1,2} \left(\frac{\beta_B^2 P_s}{N_o} x^2 \mid \begin{matrix} 0, 0 \\ 0, -1 \end{matrix} \right) \times G_{0,2}^{2,0} \left(\Xi^2 x^2 \mid \frac{k_A-m_A}{2}, -\frac{k_A-m_A}{2} \right) dx. \quad (36)$$

By setting $y = x^2$, (36) can be written as

$$\mathcal{J} = \frac{\beta_B^2 P_s}{4\ln(2) N_o} \int_0^\infty y^{\frac{1}{2}(k_A+m_A)} G_{2,2}^{1,2} \left(\frac{\beta_B^2 P_s}{N_o} y \mid \begin{matrix} 0, 0 \\ 0, -1 \end{matrix} \right) \times G_{0,2}^{2,0} \left(\Xi^2 y \mid \frac{k_A-m_A}{2}, -\frac{k_A-m_A}{2} \right) dy. \quad (37)$$

By applying [31, ch. 2.3], (37) can be expressed as

$$\mathcal{J} = \frac{1}{4\ln(2)} \left(\frac{\beta_B^2 P_s}{N_o} \right)^{-\frac{k_A+m_A}{2}} \times G_{2,4}^{4,1} \left(\frac{\Xi^2 N_o}{\beta_B^2 P_s} \mid \frac{k_A-m_A}{2}, -\frac{k_A-m_A}{2}, 1 - \frac{k_A+m_A}{2}, -\frac{k_A+m_A}{2} \right). \quad (38)$$

With the aid of (38), (32) can be rewritten as

$$\bar{C}_B = \frac{1}{\ln(2)} \left(\frac{\beta_B^2 P_s}{N_o} \right)^{-\frac{k_A+m_A}{2}} \frac{\Xi^{k_A+m_A}}{\Gamma(k_A)\Gamma(m_A)} \times G_{2,4}^{4,1} \left(\frac{\Xi^2 N_o}{\beta_B^2 P_s} \mid \frac{k_A-m_A}{2}, -\frac{k_A-m_A}{2}, 1 - \frac{k_A+m_A}{2}, -\frac{k_A+m_A}{2} \right). \quad (39)$$

The ergodic capacity of the eavesdropping channel can be computed as

$$\bar{C}_E = \int_0^\infty \log_2 \left(1 + \frac{\beta_E^2 P_s}{N_o} x^2 \right) f_{h_E}(x) dx, \quad (40)$$

which, by applying (9), can be rewritten as

$$\bar{C}_E = \sum_{l=1}^L 2a_l^{(3)} \mathcal{K}_l, \quad (41)$$

where

$$\mathcal{K}_l = \int_0^\infty x^{2b_l^{(3)}-1} \exp(-c_3 x^2) \log_2 \left(1 + \frac{\beta_E^2 P_s}{N_o} x^2 \right) dx, \quad (42)$$

which can be rewritten as

$$\mathcal{K}_l = \frac{1}{\ln(2)} \int_0^\infty x^{2b_l^{(3)}-1} \exp(-c_3 x^2) \times \ln \left(1 + \frac{\beta_E^2 P_s}{N_o} x^2 \right) dx. \quad (43)$$

By setting $z = x^2$, (43)

$$\mathcal{K}_l = \frac{1}{2\ln(2)} \int_0^\infty z^{b_l^{(3)}-1} \exp(-c_3 z) \times \ln \left(1 + \frac{\beta_E^2 P_s}{N_o} z \right) dz, \quad (44)$$

which, by applying [23, Eq. (8.352/2)], can be rewritten as

$$\mathcal{K}_l = \frac{1}{2\ln(2)} \int_0^\infty z^{b_l^{(3)}-1} \exp(-c_3 z) \times G_{2,2}^{1,2} \left(\frac{\beta_E^2 P_s}{N_o} z \mid \begin{matrix} 0, 0 \\ 0, -1 \end{matrix} \right) dz. \quad (45)$$

Moreover, with the aid of [23, Eq. (8.352/2)], (45) can be expressed as

$$\mathcal{K}_l = \frac{1}{2\ln(2)} \int_0^\infty z^{b_l^{(3)}-1} \Gamma(1, c_3 z) \times G_{2,2}^{1,2} \left(\frac{\beta_E^2 P_s}{N_o} z \mid \begin{matrix} 0, 0 \\ 0, -1 \end{matrix} \right) dz, \quad (46)$$

which, by applying [24, Eq. (15.1.1)] and [23, Eq. (9.34/7)], yields

$$\mathcal{K}_l = \frac{1}{2\ln(2)} \int_0^\infty z^{b_l^{(3)}-1} G_{1,2}^{2,0} \left(c_3 z \mid \begin{matrix} 1 \\ 0, 1 \end{matrix} \right) \times G_{2,2}^{1,2} \left(\frac{\beta_E^2 P_s}{N_o} z \mid \begin{matrix} 0, 0 \\ 0, -1 \end{matrix} \right) dz. \quad (47)$$

With the aid of [31, ch. 2.3], (47) can be rewritten as

$$\mathcal{K}_l = \frac{c_3^{-b_l^{(3)}}}{2\ln(2)} G_{4,3}^{1,4} \left(\frac{\beta_E^2 P_s}{c_3 N_o} \mid \begin{matrix} 0, 0, 1 - b_l^{(3)}, -b_l^{(3)} \\ 0, -b_l^{(3)}, -1 \end{matrix} \right) \quad (48)$$

By applying (48) in (41), we obtain

$$\bar{C}_E = \sum_{l=1}^L \frac{a_l^{(3)} c_3^{-b_l^{(3)}}}{\ln(2)} \times G_{4,3}^{1,4} \left(\frac{\beta_E^2 P_s}{c_3 N_o} \mid \begin{matrix} 0, 0, 1 - b_l^{(3)}, -b_l^{(3)} \\ 0, -b_l^{(3)}, -1 \end{matrix} \right). \quad (49)$$

Finally, with the aid of (39) and (49), (29) can be written as in (15). This concludes the proof.

REFERENCES

- [1] A.-A. A. Boulogeorgos, J. M. Jornet, and A. Alexiou, "Directional terahertz communication systems for 6G: Fact check," *IEEE Veh. Technol. Mag.*, vol. 16, no. 4, pp. 68–77, Dec. 2021.
- [2] Z. Wan, Z. Gao, F. Gao, M. D. Renzo, and M.-S. Alouini, "Terahertz massive MIMO with holographic reconfigurable intelligent surfaces," *IEEE Trans. Commun.*, vol. 69, no. 7, pp. 4732–4750, Jul. 2021.
- [3] T. A. Tsiftsis, C. Valagiannopoulos, H. Liu, A.-A. A. Boulogeorgos, and N. I. Miridakis, "Metasurface-coated devices: A new paradigm for energy-efficient and secure 6g communications," *IEEE Veh. Technol. Mag.*, vol. 17, no. 1, pp. 27–36, Mar. 2022.
- [4] K. Ntontin, A.-A. A. Boulogeorgos, D. G. Selimis, F. I. Lazarakis, A. Alexiou, and S. Chatzinotas, "Reconfigurable intelligent surface optimal placement in millimeter-wave networks," *IEEE Open Journal of the Communications Society*, vol. 2, pp. 704–718, 2021.
- [5] A.-A. Boulogeorgos, N. D. Chatzidiamantis, H. Sandalidis, A. Alexiou, and M. D. Renzo, "Cascaded composite turbulence and misalignment: Statistical characterization and applications to reconfigurable intelligent surface-empowered wireless systems," *IEEE Trans. Veh. Technol.*, vol. 71, no. 4, pp. 3821–3836, Apr. 2022.
- [6] K. Ntontin, A.-A. A. Boulogeorgos, E. Bjornson, W. A. Martins, S. Kisseleff, S. Abadal, E. Alarcon, A. Papazafeiropoulos, F. Lazarakis, and S. Chatzinotas, "Wireless energy harvesting for autonomous reconfigurable intelligent surfaces," *IEEE Transactions on Green Communications and Networking*, pp. 1–1, 2022.
- [7] A.-A. A. Boulogeorgos and A. Alexiou, "Ergodic capacity analysis of reconfigurable intelligent surface assisted wireless systems," in *IEEE 3rd 5G World Forum (5GWF)*, Sep. 2020.
- [8] S. Zhang, H. Zhang, B. Di, Y. Tan, M. D. Renzo, Z. Han, H. V. Poor, and L. Song, "Intelligent omni-surfaces: Ubiquitous wireless transmission by reflective-refractive metasurfaces," *IEEE Trans. Wireless Commun.*, vol. 21, no. 1, pp. 219–233, Jan. 2022.
- [9] M. D. Renzo, A. Zappone, M. Debbah, M.-S. Alouini, C. Yuen, J. de Rosny, and S. Tretjakov, "Smart radio environments empowered by reconfigurable intelligent surfaces: How it works, state of research, and the road ahead," *IEEE J. Select. Areas Commun.*, vol. 38, no. 11, pp. 2450–2525, Nov. 2020.
- [10] W. Tang, M. Z. Chen, X. Chen, J. Y. Dai, Y. Han, M. D. Renzo, Y. Zeng, S. Jin, Q. Cheng, and T. J. Cui, "Wireless communications with reconfigurable intelligent surface: Path loss modeling and experimental measurement," *IEEE Trans. Wireless Commun.*, vol. 20, no. 1, pp. 421–439, Jan. 2021.
- [11] F. H. Danufane, M. D. Renzo, J. de Rosny, and S. Tretjakov, "On the path-loss of reconfigurable intelligent surfaces: An approach based on green's theorem applied to vector fields," *IEEE Trans. Commun.*, vol. 69, no. 8, pp. 5573–5592, Aug. 2021.
- [12] M. Cui, G. Zhang, and R. Zhang, "Secure wireless communication via intelligent reflecting surface," vol. 8, no. 5, pp. 1410–1414, Oct. 2019.
- [13] Z. Chu, W. Hao, P. Xiao, and J. Shi, "Intelligent reflecting surface aided multi-antenna secure transmission," vol. 9, no. 1, pp. 108–112, Jan. 2020.
- [14] H. Shen, W. Xu, S. Gong, Z. He, and C. Zhao, "Secrecy rate maximization for intelligent reflecting surface assisted multi-antenna communications," *IEEE Commun. Lett.*, vol. 23, no. 9, pp. 1488–1492, Sep. 2019.
- [15] S. Hong, C. Pan, H. Ren, K. Wang, K. K. Chai, and A. Nallanathan, "Robust transmission design for intelligent reflecting surface-aided secure communication systems with imperfect cascaded CSI," *IEEE Trans. Wireless Commun.*, vol. 20, no. 4, pp. 2487–2501, Apr. 2021.
- [16] Y. Sun, K. An, Y. Zhu, G. Zheng, K.-K. Wong, S. Chatzinotas, H. Yin, and P. Liu, "RIS-assisted robust hybrid beamforming against simultaneous jamming and eavesdropping attacks," *IEEE Trans. Wireless Commun.*, pp. 1–1, Jul. 2022.
- [17] L. Yang, J. Yang, W. Xie, M. O. Hasna, T. Tsiftsis, and M. D. Renzo, "Secrecy performance analysis of RIS-aided wireless communication systems," *IEEE Trans. Veh. Technol.*, vol. 69, no. 10, pp. 12 296–12 300, Oct. 2020.
- [18] P. Xu, G. Chen, G. Pan, and M. D. Renzo, "Ergodic secrecy rate of RIS-assisted communication systems in the presence of discrete phase shifts and multiple eavesdroppers," vol. 10, no. 3, pp. 629–633, Mar. 2021.
- [19] L. Lv, Q. Wu, Z. Li, N. Al-Dhahir, and J. Chen, "Secure two-way communications via intelligent reflecting surfaces," *IEEE Commun. Lett.*, vol. 25, no. 3, pp. 744–748, Mar. 2021.
- [20] I. Trigui, W. Ajib, and W.-P. Zhu, "Secrecy outage probability and average rate of RIS-aided communications using quantized phases," *IEEE Commun. Lett.*, vol. 25, no. 6, pp. 1820–1824, Jun. 2021.
- [21] Y. Ai, F. A. P. de Figueiredo, L. Kong, M. Cheffena, S. Chatzinotas, and B. Ottersten, "Secure vehicular communications through reconfigurable intelligent surfaces," *IEEE Trans. Veh. Technol.*, vol. 70, no. 7, pp. 7272–7276, Jul. 2021.
- [22] A.-A. A. Boulogeorgos, A. Alexiou, and M. D. Renzo, "Outage performance analysis of RIS-assisted UAV wireless systems under disorientation and misalignment," *IEEE Trans. Veh. Technol.*, pp. 1–16, Jul. 2022.
- [23] I. S. Gradshteyn and I. M. Ryzhik, *Table of Integrals, Series, and Products*, 6th ed. New York: Academic, 2000.
- [24] M. Abramowitz and I. A. Stegun, *Handbook of Mathematical Functions with Formulas, Graphs, and Mathematical Tables*. New York: Dover Publications, 1965.
- [25] A.-A. A. Boulogeorgos and A. Alexiou, "Performance analysis of reconfigurable intelligent surface-assisted wireless systems and comparison with relaying," vol. 8, pp. 94 463–94 483, 2020.
- [26] —, "Coverage analysis of reconfigurable intelligent surface assisted THz wireless systems," *IEEE Open Journal of Vehicular Technology*, vol. 2, pp. 94–110, 2021.
- [27] L. Dai, B. Wang, M. Wang, X. Yang, J. Tan, S. Bi, S. Xu, F. Yang, Z. Chen, M. D. Renzo, C.-B. Chae, and L. Hanzo, "Reconfigurable intelligent surface-based wireless communications: Antenna design, prototyping, and experimental results," *IEEE Access*, vol. 8, pp. 45 913–45 923, 2020.
- [28] Y. Liu, X. Liu, X. Mu, T. Hou, J. Xu, M. D. Renzo, and N. Al-Dhahir, "Reconfigurable intelligent surfaces: Principles and opportunities," *IEEE Commun. Surveys Tuts.*, vol. 23, no. 3, pp. 1546–1577, 2021.
- [29] S. Lin, B. Zheng, G. C. Alexandropoulos, M. Wen, M. D. Renzo, and F. Chen, "Reconfigurable intelligent surfaces with reflection pattern modulation: Beamforming design and performance analysis," *IEEE Trans. Wireless Commun.*, vol. 20, no. 2, pp. 741–754, Feb. 2021.
- [30] Wolfram Research, Inc., "functions.wolfram.com/03.04.26.0006.01," <http://functions.wolfram.com/03.04.26.0006.01>, Oct. 2001, accessed: 08/07/2022.
- [31] A. M. Mathaia, R. K. Saxena, and H. J. Haubold, Eds., *The H-Function: Theory and Applications*. London. U.K.: Springer, 2010.